The impact of anthropometric patient-phantom matching on organ dose: A hybrid phantom study for fluoroscopy guided interventions

Perry B. Johnson, Amy Geyer, David Borrego, and Kayla Ficarrotta
Nuclear and Radiological Engineering, University of Florida, Gainesville, Florida 32611

Kevin Johnson
Radiology, University of Florida, Jacksonville, Florida 32209

Wesley E. Bolch[a)]
Department of Nuclear and Radiological/Biomedical Engineering, University of Florida, Gainesville, Florida 32611-8300

(Received 1 October 2010; revised 22 December 2010; accepted for publication 23 December 2010; published 31 January 2011)

Purpose: To investigate the benefits and limitations of patient-phantom matching for determining organ dose during fluoroscopy guided interventions.
Methods: In this study, 27 CT datasets representing patients of different sizes and genders were contoured and converted into patient-specific computational models. Each model was matched, based on height and weight, to computational phantoms selected from the UF hybrid patient-dependent series. In order to investigate the influence of phantom type on patient organ dose, Monte Carlo methods were used to simulate two cardiac projections (PA/left lateral) and two abdominal projections (RAO/LPO). Organ dose conversion coefficients were then calculated for each patient-specific and patient-dependent phantom and also for a reference stylized and reference hybrid phantom. The coefficients were subsequently analyzed for any correlation between patient-specificity and the accuracy of the dose estimate. Accuracy was quantified by calculating an absolute percent difference using the patient-specific dose conversion coefficients as the reference.
Results: Patient-phantom matching was shown most beneficial for estimating the dose to heavy patients. In these cases, the improvement over using a reference stylized phantom ranged from approximately 50% to 120% for abdominal projections and for a reference hybrid phantom from 20% to 60% for all projections. For lighter individuals, patient-phantom matching was clearly superior to using a reference stylized phantom, but not significantly better than using a reference hybrid phantom for certain fields and projections.
Conclusions: The results indicate two sources of error when patients are matched with phantoms: Anatomical error, which is inherent due to differences in organ size and location, and error attributed to differences in the total soft tissue attenuation. For small patients, differences in soft tissue attenuation are minimal and are exceeded by inherent anatomical differences. For large patients, difference in soft tissue attenuation can be large. In these cases, patient-phantom matching proves most effective as differences in soft tissue attenuation are mitigated. With increasing obesity rates, overweight patients will continue to make up a growing fraction of all patients undergoing medical imaging. Thus, having phantoms that better represent this population represents a considerable improvement over previous methods. In response to this study, additional phantoms representing heavier weight percentiles will be added to the UFHADM and UFHADF patient-dependent series. [DOI: 10.1118/1.3544353]

Key words: reference phantoms, hybrid phantoms, organ dosimetry, fluoroscopy, radiology, patient dosimetry

I. INTRODUCTION

Since first being used in 1999 as a developmental tool for the NCAT heart phantom,[1] computer animation software has become the standard for creating the next generation of anthropomorphic computational phantoms. Programs such as RHINOCEROS (McNeel North America, Seattle, WA), 3D DOCTOR (Able Software Corp., Lexington, MA), BLENDER,[2] AUTODESK MAYA (Autodesk, Toronto, Canada), and MAKEHUMAN[3] have all been used to create a variety of NURBS and mesh-based models of human anatomy for radiation dose assessment.[4–7] These models share the advantages of animation software including the ability to modify posture, organ size, organ location, and total body shape, while at the same time maintaining anatomical accuracy. This wide-ranging adaptability provides a means to more accurately represent individual patients, a major shift from previous convention that relied heavily on standardized reference phantoms and their efficacy for dosimetry across large patient populations.

Animation-based phantoms allow for increased patient specificity through the development of patient-dependent

phantoms and the process of patient-phantom matching. In the previous work by the authors, the concept of a patient-dependent phantom was first introduced.[8,9] This phantom category consists of off-the-shelve models created through anthropometric remodeling of a reference phantom. The goal of modification is to create a library of phantoms representing a variety of different body shapes and contours as might be seen in a real patient population. Patient-phantom matching is then defined as the selection of a patient-dependent phantom or patient-dependent dose metric based on anthropometric measurement of an individual patient. The primary benefit is the balance between specificity and practicality. Previously, tomographic-based phantoms have provided high-specificity, but as a trade-off, require large sets of imaging data and time-consuming segmentation. Conversely, reference phantoms provide an off-the-shelve solution but ignore anatomic and anthropometric variability. By using patient-phantom matching, patient information can be included in a near-real time dose estimate, thus opening the possibility for individual dose tracking.

While patient-phantom matching represents an obvious extension for animation-based phantoms, the question remains as to whether or not anthropometric matching can actually improve dose estimates to individual patients. In previous studies of organ doses, an increased body diameter, body mass index, and weight percentile were all shown to increase organ dose for a given image quality.[8,10,11] These results suggest that having a larger phantom to represent a larger patient would help mitigate dosimetric differences due to body morphometry. Beyond these studies, little work has been published comparing phantoms and patients of different sizes for projection-based radiology (fluoroscopy and radiography).

Another important aspect of patient-phantom matching independent of patient size is the inherent variability in organ size, shape, and location. Such variability introduces uncertainty into any dose estimate and this is important to consider when assessing the effectiveness of matching techniques. One notable study performed by Zankl *et al.*[12] provided an intercomparison between seven different tomographic-based models (Donna, Irene, Frank, Helga, Golem, Voxelman, and Visible Human). The study had several interesting findings. First, the influence of individual anatomy was found most relevant for incident photon energies between 60 and 200 keV. Below this range, even small individual variations, both anthropometric and anatomical, produced dose differences of hundreds of percent. Above this range, the penetration and scatter of the photon beam was relatively high, thus lessening the effects of individual organ variations. Second, by comparing voxelized organ volumes between the Visible Human and VIP-Man, which were both segmented from the same dataset, the study concluded that segmentation could account for errors up to 15% for large organs and 25%–60% for small and walled organs. Finally, the authors found dose differences between phantoms ranged up to 30% for organs located at shallow depths and within the field of view (FOV). For deep-seated organs or those outside the FOV, differences in organ doses ranged from 30% to 100%. While anthropometric differences accounted for part of this error (Irene was thin, while Visible Human, Frank, and Helga were larger), the results suggest a residual limitation due to anatomical (organ-related) differences. This theory will be discussed later and in more detail in this study.

While the aforementioned study included seven different patient-specific or semi-patient-specific models, it was clearly limited by sample size. Also, the purpose of the study was not to test patient-phantom matching, but to investigate systematic differences when compared to older stylized phantoms. In order to provide a comprehensive analysis of patient-phantom matching, two robust sets of phantoms are needed: One consisting of patient-specific models and the other consisting of a patient-dependent library. In this present study, both phantom sets have been compiled and include 27 patient-specific models created through CT segmentation and 50 patient-dependent phantoms selected from the UF hybrid adult male (UFHADM) and female (UFHADF) patient-dependent series.[9] Assuming the patient-specific models as a "gold standard," the hypothesis for this research was that patient-phantom matching using hybrid patient-dependent phantoms would produce more accurate organ dose estimates than those determined using reference phantoms. The study was focused on projection-based radiology, specifically dose conversion coefficients used in fluoroscopically guided interventions.

II. METHODS AND MATERIALS

To begin the study, 27 CT datasets (14 male/13 female) were retrieved from the PACS archives at Shands Jacksonville Medical Center under an approved IRB protocol. The datasets covered the chest, abdomen, and pelvic (CAP) regions and were selected preferentially so as to cover broad ranges of height and weight. In order to create a computational model for each patient, the CT datasets were contoured using the segmentation software 3D DOCTOR. As it was difficult to delineate certain soft tissue organs such as the colon and small intestine, the following organs/structures were chosen as targets for this study: The pericardium, liver, spleen, stomach (wall and contents), pancreas, kidneys, bladder (wall and contents), skeleton, subcutaneous fat, and outer body contour. After all structures of a given dataset were contoured, the model was imported as a polygon mesh into the computer animation software RHINOCEROS. Due to the fact that the CAP scans often included two separate datasets (abdomen/pelvis and chest), each half of the patient-specific phantoms was aligned properly within RHINOCEROS. Following this adjustment and a quick anatomical review, the phantoms were voxelized at a resolution of $2\times2\times2$ mm^3 and converted into a MCNPX lattice structure.

Figures 1(a) and 1(b) show height and weight information for the patient-specific phantoms overlaid on a plot of standing height versus weight for the male and female UF hybrid adult patient-dependent series, respectively. The two series, consisting of 25 male and 25 female phantoms,[9] were designed specifically for the U.S. adult population based on anthropometric data retrieved from the NHANES III exami-

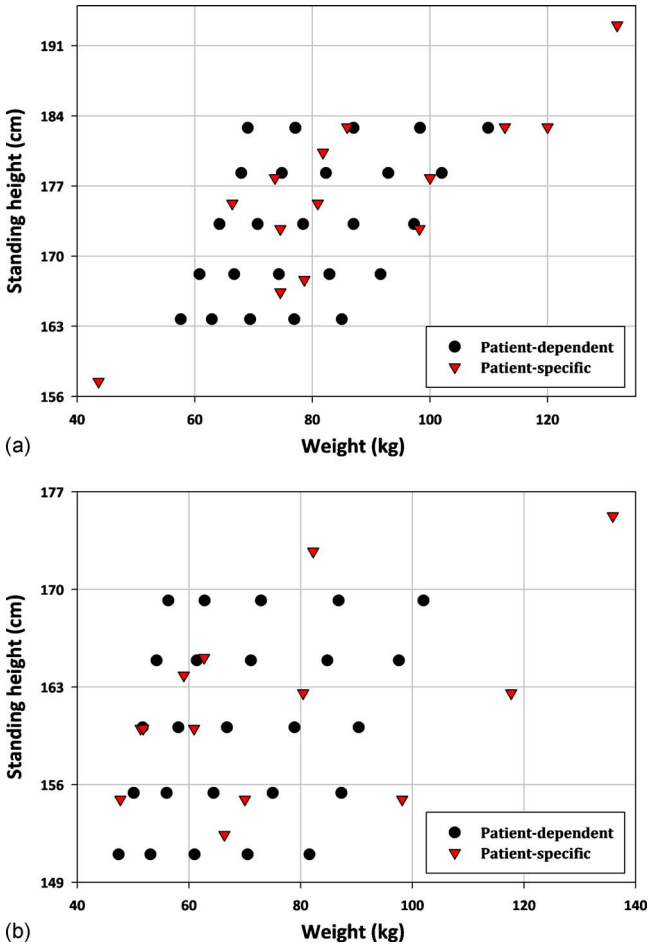

FIG. 1. Patient standing height versus weight shown for patient-dependent and patient-specific (a) male and (b) female phantoms.

nation data file.[13] This database, compiled by the National Center for Health Statistics of the Centers for Disease Control and Prevention, includes anthropometric data for roughly 34 000 individuals and was used to parametrize several measurements including standing height, sitting height, total body mass, arm circumference, waist circumference, buttock circumference, and thigh circumference. From the parametrization, 25 distinct male and female phantoms were created by modifying the UF hybrid adult male and female reference phantoms. The phantoms for each gender were created at five different height percentiles (10th, 25th, 50th, 75th, and 90th), and within each height percentile, at five different weight percentiles (10th, 25th, 50th, 75th, and 90th). As can be seen in the figures, the selected patients cover these ranges fairly well and also include a number of outliers representing body types outside the 10th and 90th percentile bounds.

In order to make a consistent comparison with the patient-specific models, each patient-dependent phantom was manually modified within the modeling program RHINOCEROS in three ways. First, the arms, legs, and head were removed in accordance with the information available in the CAP datasets. Second, organs and structures not contoured in the patient-specific models were removed. These included the costal cartilage, intestines, and prostate among others. The

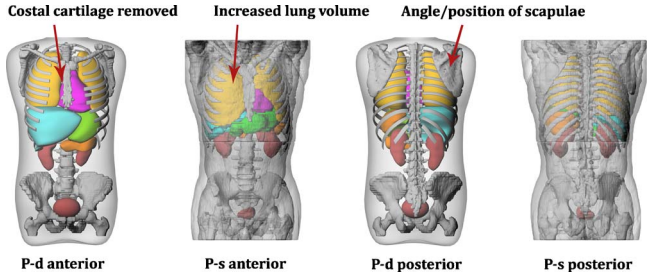

FIG. 2. Patient-dependent (P-d) phantoms were modified to match the contoured patient-specific (P-s) datasets. Modification included the removal of cartilage, intestines, and prostate among others, and the rotation of the scapulae to mimic an arms-raised positioning. The increased lung volume of the patient-specific phantoms due to breath-holding techniques is also highlighted.

final modification was to adjust the angle of the scapulae to mimic the arms-raised positioning of a real CT setup. Figure 2 illustrates a modified patient-dependent phantom shown alongside a patient-specific model. While every effort was made to normalize the patient-dependent phantoms, as seen in the figure, differences due to variable filling of the lung, bladder, and stomach were not addressed. This limitation will be discussed in further sections of this study. As with the patient-specific models, the modified phantoms were voxelized at a resolution of $2\times2\times2$ mm^3 and converted into an MCNPX lattice structure.

With both phantom libraries compiled, four different fluoroscopic projections were simulated using the radiation transport code MCNPX 2.6.0.[14] The projections included two abdominal studies centered on the stomach, LPO/RAO, and two cardiac studies centered on the heart, PA/left lateral. For the purposes of this study, all projections were viewed from the perspective of the x-ray tube. As an example, an LPO projection indicates that x rays enter the body on the patient's left-posterior side. Details regarding field size, source distance, and beam quality were taken from organ dose handbooks compiled by the Center for Devices and Radiological Health (CDRH) of the FDA.[15,16] These parameters were then modified slightly to account for differences in phantom sizing. For abdominal projections, the field of view at the detector was set to 11.5×11.5 cm^2. This was done by simulating an adjustable lead collimator located 10 cm from the source term. The source-to-skin distance was fixed at 50 cm, and the detector was positioned roughly 6–7 cm away from the patient. For cardiac projections, the field of view was set to 6.5×6.5 and 10×10 cm^2 for the left lateral and PA projections, respectively. The source-to-skin distance was fixed at 50 cm, and the detector was positioned 10 cm from the patient. In order to simplify the simulations, both the phantom and the collimator were located within an air-filled medium without the addition of a table or mattress.

Three diagnostic x-ray spectra were simulated for each projection using the SPEC 78 spectrum generator[17] and parameters taken from the CDRH dose handbooks. For abdominal projections, peak voltages were set at 80, 100, and 120 kVp. Tungsten was used as a target material with an anode angle of 12° and filtration/half-value layers set at 4.0/

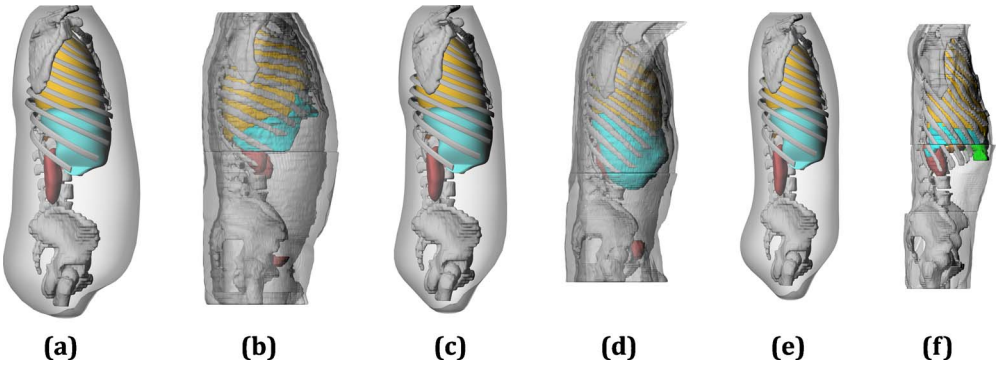

FIG. 3. Patient-phantom matching by height and weight where the closest patient-dependent phantom is shown for three different adult male patients. [(a) and (b), large] Patient-dependent 90th percentile by height/90th percentile by weight, 182.9 cm/110.0 kg—Patient-specific 182.9 cm/112.7 kg. [(c) and (d), medium] Patient-dependent 75th/50th, 178.3 cm/82.3 kg—Patient-specific 175.2 cm/80.9 kg. [(e) and (f), small] Patient-dependent 10th/10th, 163.7 cm/57.6 kg—Patient-specific 157.5 cm/43.6 kg.

4.8, 4.7/5.0, and 3.8/5.5 mm Al, respectively. For cardiac projections, peak voltages were set at 60, 90, and 120 kVp. Tungsten was again used as the target material with the filtration/half-value layers set at 3.5/2.5, 4.0/4.1, and 4.3/5.8 mm Al. The total number of phantoms used in this study as 78—27 patient-specific, 50 patient-dependent, and 1 reference stylized phantom.[18] For each phantom, the *F*6 tally (MeV g^{-1}) was used to estimate dose to the eight organs listed previously. This tally provided an estimation of kerma, which was used as an analog for absorbed dose in this study. The tallies were further normalized by dose-area-product (DAP), which was simulated using a 1 cm thick rectangular air-filled volume located 10 cm from the collimator. An entrance side metric was chosen to mimic how organ dose is calculated in the clinic; DAP is first measured during the procedure, and dose conversion coefficients (dose/DAP or DCC) are then selected from published values. Besides providing an entrance side normalization factor, the DAP was used as a convenient check on the simulation as the DAP calculated for each phantom should be similar for a given projection/spectrum combination. The Monte Carlo simulations were run on the ALRADS cluster at UF comprised of 9 AMD Dual Opteron 2216 processors with 4 GB of RAM and 4 AMD Quad Opteron 2350 processors with 8 GB of RAM. All runs included 10 million photon histories and generally took between 400 and 700 min each. The number of histories was sufficient such that the relative error was reduced below 1% for all organs, except the bladder which ranged between 1% and 10%.

After the simulations were completed, the dose conversion coefficients were analyzed for any correlation between patient-specificity and accuracy of the dose estimate. This was done by comparing the conversion coefficients calculated from a reference stylized phantom, the reference hybrid phantom (50th percentile by height and weight), and a matched patient-dependent phantom to the conversion coefficients calculated from each patient-specific model. To assist the matching process, a surface plot was created for each organ based on the height, weight, and magnitude of the dose conversion coefficient as calculated from the 25 male and 25 female patient-dependent phantoms. Matching was then performed according to height and weight where interpolation along the surface plot was used whenever the anthropometric parameters of the patient-specific model did not agree closely with one of the defined patient-dependent phantoms. Figure 3 displays a large, medium, and small individual shown with their closest patient-dependent counterpart. The figure provides a good illustration of how patient-dependent phantoms can more accurately describe a variable patient population. It is important to remember, however, that matching was performed using interpolation between patient-dependent dose metrics, which allowed for more than a one-to-one complement.

Accuracy was quantified for each phantom type by calculating an absolute percent difference using the patient-specific dose conversion coefficients as the true value. This method of calculating percent difference is defined in Eqs. (1)–(3),

$$\text{Percent difference}_{\text{Patient-dependent}} = \frac{|\text{DCC}_{\text{Patient-dependent}} - \text{DCC}_{\text{Patient-specific}}|}{\text{DCC}_{\text{Patient-specific}}}, \quad (1)$$

$$\text{Percent difference}_{\text{Reference hybrid}} = \frac{|\text{DCC}_{\text{Reference hybrid}} - \text{DCC}_{\text{Patient-specific}}|}{\text{DCC}_{\text{Patient-specific}}}, \quad (2)$$

$$\text{Percent difference}_{\text{Reference stylized}} = \frac{|\text{DCC}_{\text{Reference stylized}} - \text{DCC}_{\text{Patient-specific}}|}{\text{DCC}_{\text{Patient-specific}}}. \quad (3)$$

A percentage point improvement was also utilized, as defined in Eqs. (4) and (5),

$$\text{Percentage point}_{\text{Hybrid}} = (\text{Percent difference}_{\text{Reference hybrid}} - \text{Percent difference}_{\text{Patient-dependent}}), \quad (4)$$

TABLE I. Mean organ volumes as contoured from 14 male and 13 female CT datasets. Reference organ volumes are also listed for the 50th percentile by weight/50th percentile by mass UFHADM and UFHADF and for the reference stylized model.

	Male—Mean organ volume (cm^3)			Female—Mean organ volume (cm^3)		
	Patient-specific	Reference hybrid	Reference stylized	Patient-specific	Reference hybrid	Reference stylized
Lung	4681.6	3199.1	3370.0	3769.8	2659.4	3370.0
Liver	1763.3	1715.8	1830.0	1603.3	1252.5	1830.0
Pericardium	824.4	802.5	740.0	614.0	557.2	740.0
Stomach	476.0	447.3	402.0	362.7	374.9	402.0
Kidneys	426.8	312.8	288.0	311.0	261.5	288.0
Spleen	418.5	142.9	144.0	179.3	116.5	144.0
Bladder	145.8	250.2	249.0	195.8	189.3	249.0
Pancreas	45.7	137.3	117.0	35.7	111.6	117.0
Mean height (cm^2)	175.8	173.2	170.0	161.4	160.1	170.0
Mean weight (kg)	87.4	78.4	75.0	75.7	66.8	75.0

$$\text{Percentage point}_{\text{Stylized}} = (\text{Percent difference}_{\text{Reference stylized}} - \text{Percent difference}_{\text{Patient-dependent}}). \quad (5)$$

III. RESULTS

Mean organ volumes as segmented from the patient-specific CT datasets are listed in Table I. Reference volumes are also listed for the UFHADM, UFHADF, and reference stylized phantoms. The expectation was to see organ volumes close to or slightly higher than the reference volumes as both the mean height and the weight of the male and female datasets were greater than their corresponding reference values. As shown in Table I, several organs matched closely with this expectation including the male liver, pericardium, stomach, and kidneys, and female liver, pericardium, stomach, kidneys, spleen, and bladder. In both the male and the female cases, the lung volumes were greater by approximately 40%. In addition to differences in phantom sizing, this discrepancy was most likely due to the expanded lung volumes of patients undergoing CT scans where a breath-hold is required in order to avoid motion blur. Three organs, the male and female pancreas and the male spleen, did not agree closely with expectation. While differences in pancreas volume can be explained by segmentation error (this organ was notoriously difficult to visualize in the CT images), the spleen was clearly visible and contoured appropriately in the female datasets. After reviewing dictation notes for the male patients, in only 9 out of 14 cases was the spleen noted as having a normal appearance. In three cases, splenomegaly was specifically identified. No information was given for the remaining two patients. These findings agree with observations from the contoured datasets, and as a result, the mean spleen volume was increased higher than what would be expected in a normal patient population. With the exception of these two cases, however, the organ volumes for the male and female patient-specific models were found within normal bounds.

As mentioned previously, 78 phantoms were used in this study with 12 different Monte Carlo runs performed for each phantom. Dose conversion coefficients were calculated for each organ and an absolute percent difference was determined for each of three phantom types: Reference stylized, reference hybrid, and patient-dependent hybrid. Table II lists these results for RAO abdominal projections where the absolute percent difference has been averaged for each male organ. The table is structured in multiple ways. First, the values are separated by tube voltage. Second, the values have been compiled into three column groups as the average of all patients, as the average of heavy patients (>50th percentile by weight), and as an average of light patients (≤50th percentile by weight). Third, at the bottom of each column, the table includes both the average of all organs and the average of organs considered primary for the projection based on the magnitude of the conversion coefficients. For RAO abdominal projections, these organs were the pericardium, stomach, pancreas, and liver. The primary organs for LPO abdominal projections were the stomach, spleen, and kidneys, for PA cardiac projections the lungs, pericardium, and spleen, and for left lateral cardiac projections the lungs, pericardium, stomach, and spleen.

The RAO abdominal projection selected for Table II highlights many of the general trends observed across all projections. It can be seen that increasing tube potential improves the accuracy of the dose estimate. This is further illustrated in Fig. 4, which shows percent differences for 80, 100, and 120 kVp RAO projections, taken as the average of all organs for all male patients. This trend was also seen, however, for individual organs of both sexes. Also shown in Fig. 4 is the magnitude of the differences between the three phantom types. In Table II, these differences are quantified where, taken as an average of all patients, the stylized phantom provided the least accurate dose estimates, while the patient-matched phantom provided the best estimate. While giving some support for the concept of patient-phantom matching, this conclusion changes slightly when patients are separated by weight. Figures 5(a) and 5(b) (male and female, respec-

TABLE II. Mean absolute percent difference for individual organs of three patient groupings, all (14 patients), heavy (5), and light (9) male patients as calculated for 80, 100, and 120 kVp RAO projections. Primary organs for RAO projects were considered to be the pericardium, stomach, pancreas, and liver.*

	Patient-matched			Reference hybrid			Reference stylized		
	All	Heavy	Light	All	Heavy	Light	All	Heavy	Light
				80 kVp					
Lung	40.8	44.1	39.0	41.0	53.9	33.8	55.9	46.3	61.2
Pericardium*	43.7	35.2	48.4	39.4	36.7	41.0	75.6	72.9	77.1
Bladder	85.1	157.1	45.1	98.9	203.2	40.9	240.1	456.1	120.2
Stomach*	32.0	43.3	25.8	36.9	50.0	29.6	56.6	108.0	28.0
Pancreas*	25.2	28.5	23.4	32.6	30.9	33.6	32.7	67.9	13.2
Liver*	29.2	32.7	27.3	51.8	96.3	27.0	46.7	36.9	52.1
Spleen	52.8	65.8	45.6	73.8	139.9	37.0	186.6	301.2	122.9
Kidneys	23.5	15.6	27.8	34.3	54.8	23.0	52.0	91.5	30.1
Average	41.6	52.8	35.3	51.1	83.2	33.2	93.3	147.6	63.1
Primary	32.5	34.9	31.2	40.2	53.5	32.8	52.9	71.4	42.6
				100 kVp					
Lung	39.1	41.5	37.7	37.7	47.1	32.5	53.8	44.6	58.9
Pericardium*	42.1	33.7	46.7	37.1	32.5	39.6	74.5	72.3	75.7
Bladder	76.5	137.1	42.8	86.4	173.0	38.4	188.7	348.9	99.7
Stomach*	29.2	39.7	23.4	33.6	44.7	27.4	49.7	92.6	25.9
Pancreas*	24.8	27.5	23.3	30.9	28.2	32.4	28.7	58.3	12.2
Liver*	27.6	30.9	25.7	47.4	86.1	25.9	46.5	36.1	52.3
Spleen	48.3	60.4	41.6	66.1	123.4	34.2	163.6	259.1	110.5
Kidneys	21.5	14.2	25.5	30.6	47.2	21.3	45.6	78.5	27.3
Average	38.6	48.1	33.3	46.2	72.8	31.5	81.4	123.8	57.8
Primary	30.9	32.9	29.8	37.2	47.9	31.3	49.8	64.8	41.5
				120 kVp					
Lung	38.2	40.2	37.1	36.2	44.1	31.8	52.8	43.8	57.9
Pericardium*	41.5	33.0	46.2	36.2	30.7	39.3	74.1	72.2	75.1
Bladder	74.3	136.0	40.0	83.3	166.7	37.0	172.4	317.0	92.0
Stomach*	28.0	37.9	22.5	32.0	42.2	26.4	46.6	85.8	24.8
Pancreas*	24.6	27.0	23.2	30.1	26.9	31.9	26.7	53.5	11.7
Liver*	26.8	30.0	25.1	45.5	81.6	25.5	46.5	35.8	52.4
Spleen	45.9	57.2	39.6	62.0	114.7	32.7	151.9	237.8	104.1
Kidneys	20.3	13.2	24.3	28.6	43.1	20.5	42.5	72.3	26.0
Average	37.5	46.8	32.3	44.2	68.7	30.6	76.7	114.8	55.5
Primary	30.2	32.0	29.3	36.0	45.3	30.7	48.4	61.8	41.0

tively) show percent difference for 80 kVp projections taken as the average of all organs for each of two groups: Heavy and light patients. In these figures, it is clearly seen that while the stylized phantom provided the least accurate dose estimate overall, patient-phantom matching was superior to using a reference hybrid phantom only for heavy patients. For light patients, the two phantom types provided an equivalent level of accuracy. Again, this trend was also seen when individual and primary organs were considered.

In order to summarize these results for the complete study, Tables III and IV list the percentage point improvement gained by using patient-phantom matching over hybrid and stylized reference phantoms, respectively. The tables are structured by tube potential, patient grouping (out of all 27 patients), and how absolute percent difference was averaged across the eight organs of interest. As seen in Figs. 5(a) and

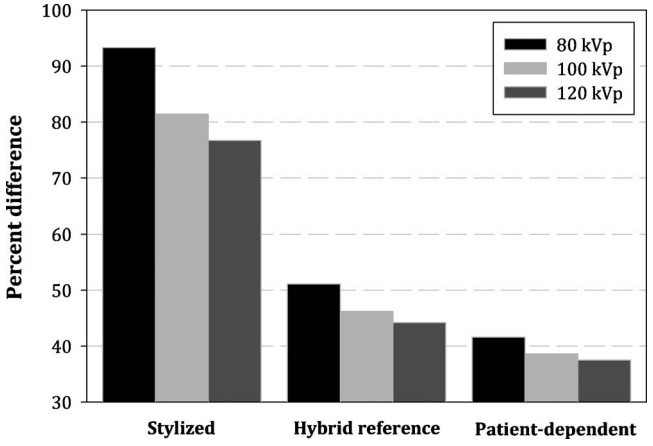

FIG. 4. Improved accuracy with increasing kVp. Shown for RAO projections as the average of all organs for all male patients.

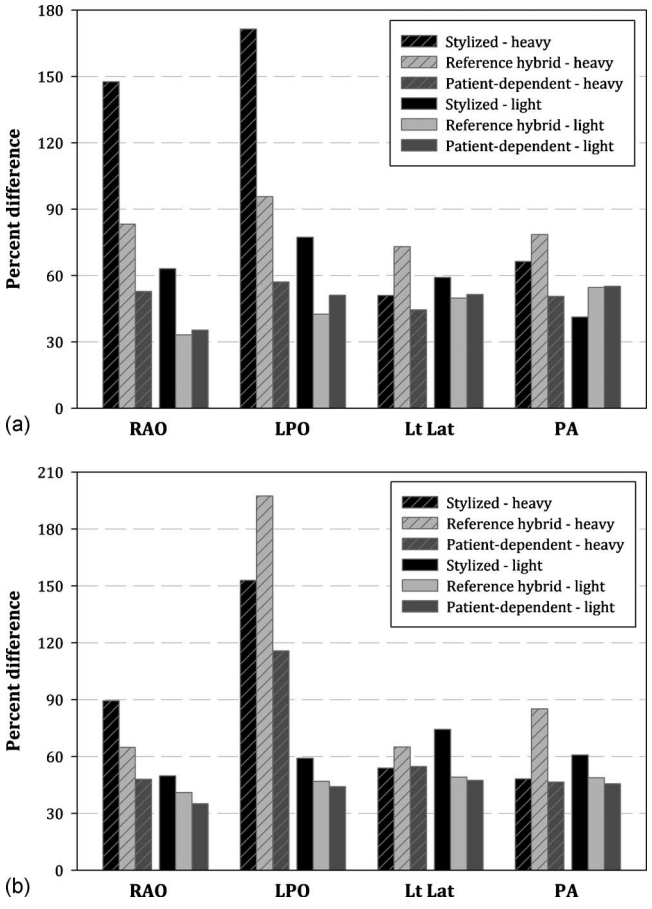

FIG. 5. (a) Improved accuracy for heavy patients, but no improvement for light patients. Shown for 80 kVp RAO, LPO, left lateral, and PA projections as the average of all organs for all male patients. (b) Improved accuracy for heavy patients, but no improvement for light patients. Shown for 80 kVp RAO, LPO, left lateral, and PA projections as the average of all organs for all female patients.

5(b) for each projection, patient-phantom matching provided significant improvement for heavy patients but little to no improvement for light patients when compared to a reference hybrid phantom. In comparison with the reference stylized phantom, patient-phantom matching provided better dose estimates for all patient groupings when abdominal studies were considered, but results varied for cardiac projections. In this case, the hybrid based phantoms provided more accurate estimates for light patients but were slightly less accurate for heavy patients.

IV. DISCUSSION

In order to further investigate dose differences between heavy and light patients, specific contour matching was performed for each of the five male patients selected from the heavy grouping. To do this, a new phantom was created for each patient using patient-dependent organs but using the patient-specific outer body contours. The phantoms were created within RHINOCEROS and subsequently used to calculate organ dose conversion coefficients for a 100 kVp LPO abdominal projection. Differences between patient-specific phantoms and the phantoms created using the patient-specific contours were quantified and are shown in Fig. 6(a) as percent difference for the average of all organs. Percent difference is also shown for the original patient-specific phantom matched to a reference phantom, matched by height to a patient-dependent phantom, and matched by height and weight. The different matching techniques are clarified graphically in Fig. 6(b).

There were several interesting findings from this comparison. For the smallest of the three "heavy" patients, a similar baseline was reached when matched by height and weight and by specific contour. For the heaviest two patients, a gradual improvement was observed for each sequential matching technique. As seen in Fig. 1, these two patients were heavier than the largest phantom selected from the

TABLE III. Percentage point improvement over a reference hybrid phantom. Primary organs were those which received the highest dose in each projection.

Abdominal		LPO			RAO		
kVp	Group	All	Heavy	Light	All	Heavy	Light
80	Average	21.0	60.1	−2.5	9.8	23.6	1.9
	Primary	26.3	70.7	−0.4	7.7	12.7	5.0
100	Average	17.2	48.9	−1.7	7.9	18.7	1.8
	Primary	21.5	56.9	0.2	6.4	10.1	4.5
120	Average	15.2	46.4	0.1	7.1	16.4	1.8
	Primary	19.4	54.4	2.6	5.9	8.9	4.2
Cardiac		Lt Lat			PA		
kVp	Group	All	Heavy	Light	All	Heavy	Light
60	Average	7.1	19.4	0.1	13.2	33.2	1.4
	Primary	9.5	25.2	0.7	17.1	39.2	4.0
90	Average	4.3	12.4	−0.2	7.5	19.0	0.6
	Primary	6.7	17.6	0.5	11.5	25.6	3.1
120	Average	3.2	9.3	−0.1	5.9	15.6	0.2
	Primary	5.6	14.7	0.3	9.7	21.0	2.9

TABLE IV. Percentage point improvement over a reference stylized phantom. Primary organs were those which received the highest dose in each projection.

Abdominal		LPO			RAO		
kVp	Group	All	Heavy	Light	All	Heavy	Light
80	Average	40.6	75.7	20.5	38.4	68.1	21.2
	Primary	60.2	121.7	24.1	23.1	36.0	15.6
100	Average	35.2	62.9	19.4	32.8	55.2	20.0
	Primary	49.2	99.0	20.0	22.0	32.2	16.1
120	Average	33.7	55.4	22.0	30.6	50.0	19.5
	Primary	46.4	93.6	22.8	21.5	30.5	16.2
Cardiac		Lt Lat			PA		
kVp	Group	All	Heavy	Light	All	Heavy	Light
60	Average	11.8	2.9	17.3	3.4	8.7	0.7
	Primary	15.0	−2.6	25.7	−2.2	−13.0	4.3
90	Average	11.8	1.6	18.1	2.7	2.5	3.1
	Primary	16.0	0.9	25.2	0.5	−7.3	5.2
120	Average	11.4	1.5	17.3	2.7	2.1	3.2
	Primary	15.6	1.9	24.0	1.5	−5.0	5.5

patient-dependent library. If a larger patient-dependent phantom had been available, a similar baseline may have been reached. By matching using a specific body contour, variation in the amount of soft tissue that shields each internal organ is mitigated. This small test indicates matching using patient height and weight has a similar effect. Further support for this theory can be deduced from Figs. 5(a) and 5(b), which show patient-phantom matching effective for heavy patients, where variation in soft tissue attenuation is large, but having little effect for light patients, where variations in soft tissue are small in comparison to the reference version.

Interestingly, Figs. 5(a) and 5(b) also reveal a baseline error of roughly 35%–45%, which was similarly observed across all projections. In the study of Zankel *et al.*,[12] comparable differences were found between the seven adult voxel models where individual anatomical variation in organs size and location was discussed as a main contributor. To test this theory, a heavy and a light patient-specific phantom were selected from the library along with their patient-dependent counterparts and rerun for a 100 kVp LPO abdominal projection with four different fields of view including 5.7×5.7, 11.5×11.5, 22.9×22.9, and 45.9×45.9 cm^2. Percent difference between patient-specific and patient-dependent phantoms was quantified as the average of all organs and is plotted in Fig. 7 for different field sizes. In each case, increasing the FOV, or effectively limiting differences in organ location,

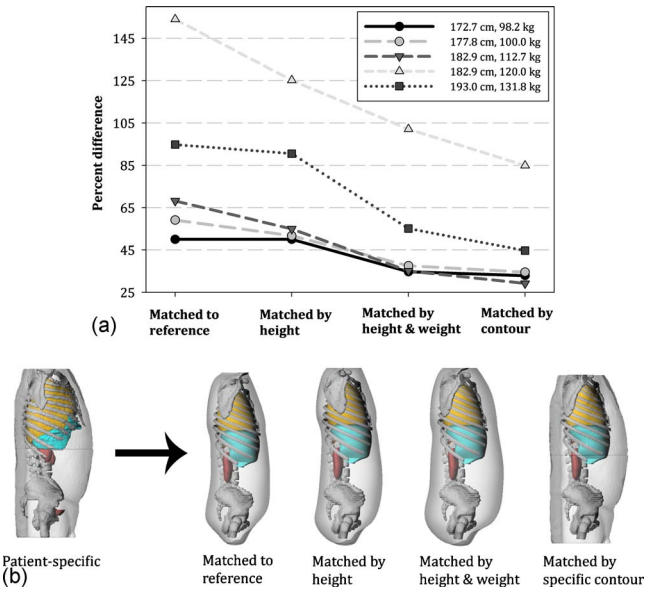

FIG. 6. (a) Percent difference for each of the five heavy male patients as matched to a reference hybrid phantom, matched by height to a patient-dependent phantom, and matched by height and weight to a patient-dependent phantom. Each phantom was also matched using a patient-specific contour but using patient-dependent organs. (b) Four different matching techniques as highlighted in (a).

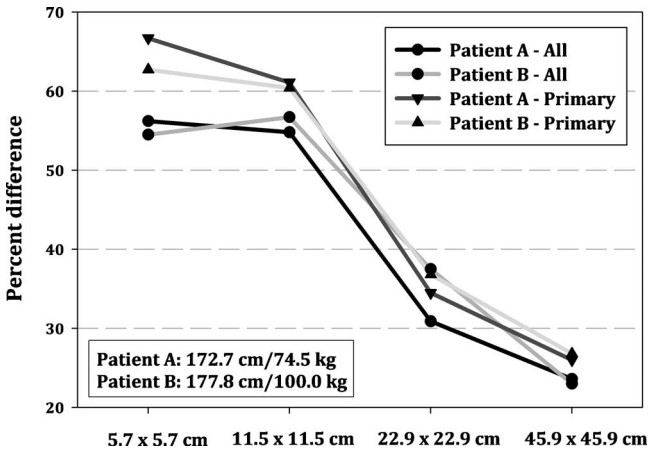

FIG. 7. Improved accuracy with increasing field of view, shown as the average of all and primary organs for two male patients.

led to a decrease in error. With an increased FOV, both the patient-specific and the patient-dependent phantoms received a more uniform fluence across each organ. An example of this would be the stomach, which was found completely within the FOV at 45.9×45.9 cm^2 but only partial within the FOV at 5.7×5.7 cm^2. Because the amount stomach found within the FOV differs between phantoms at small FOVs due to specific organ locations, the overall disagreement in organ dose is increased. This result further supports the notion that a residual limit or uncertainty is always present when patients are matched to phantoms using anthropometric parameters. This uncertainty is due to anatomical differences in organs size and location which cannot be accounted for without patient-specific imaging data.

With regard to stylized models, Table IV indicates that patient-phantom matching provides major advantages for abdominal projections and minor advantages for cardiac projections. As noted in the previous studies, stylized phantoms utilize a highly elliptical cylinder to represent the torso. The cylinder is unrealistically wide in the lateral dimension, leading to organ positions that are too peripheral.[12] Furthermore, the cross section of the cylinder remains constant with height. For abdominal projections where both the axial and the sagittal body contours are quite variable, a constant cross section introduces additional error. Patient-phantom matching reduces this error by folding patient height and weight into the dose estimate. As weight is well correlated with waist circumference, selecting a larger phantom to represent a larger patient helps reduce differences in soft tissue attenuation as mentioned previously.

For cardiac projections, the wide breadth of the cylinder actually matched better with the heavy patient grouping. As a result, the trend for light and heavy patients was reversed for left lateral projections. In this case, the stylized phantom overestimated lateral attenuation for light patients, and as a consequence, patient-phantom matching proved most beneficial for this patient class. For posterior-anterior projections, the data showed little indication of a common trend. While patient-phantom matching slightly improved accuracy when taken as the average of all organs, when only primary organs were considered, the stylized phantom exhibited better agreement with the patient-specific data. Upon further inspection, the male spleen was found as the main organ causing significant disagreement. In addition to issues mentioned previously related to the size of the male spleen, the location of the male spleen within the hybrid phantoms was found medial and superior to what was seen in both male and female patient-specific datasets. This was not the case for the female hybrid phantoms, and as a result, the female patient-dependent DCCs aligned much better with the patient-specific data. While the purpose of this study was not to verify the position of any specific organ within the UF hybrid patient-dependent series, the male spleen is an item that can be added to a list of future adjustments to better define a supine patient as most commonly seen in fluoroscopy. The list may also include the sagittal angle of the kidney, which was observed to be slightly less than what was seen in the patient images.

Beyond the anatomical differences of these organs, the expanded lung volume of the patient-specific phantoms, and the variable filling of the bladder, great effort was made to limit variables and simplify the study as much as possible in order to derive general conclusions and error trends. For this reason, the study relied on an absolute versus relative percent difference and expressed results in terms of mean values. Taken individually, organ dose as calculated using a patient-dependent phantom ranged in extreme cases from 300% high to 75% low. Using a relative percent difference would have thus underestimated the mean disagreement. While 27 patients provided enough data to compile over 900 Monte Carlo runs, the study would have benefited from a broader patient-specific dataset. With a larger library, a more thorough analysis of the dose variation to individual organs could be performed.

V. CONCLUSIONS

The purpose of this study was to investigate the effectiveness of patient-phantom matching in comparison with stylized and hybrid reference phantoms. By analyzing percent difference between actual patient dose and phantom dose, several conclusions were reached. The results indicate two sources of error when phantoms are used to represent individual patients for fluoroscopic organ dose assessment. These include uncertainty associated with variability in organs size and location, and error associated with differences in soft tissue attenuation. The first type is inherent and accounts for dosimetric differences of approximately 35%–45%. The second type depends on patient size and can be addressed using anthropometric based patient-phantom matching, specifically for large patients where error can be reduced approximately 20%–60% depending on projection. Additionally, in cases where tube potential is increased, error is further reduced as differences in organ location and patient size are lessened by a more penetrating beam.

While the results of this study indicate that patient-phantom matching is only truly useful to larger members of the patient population, obesity rates are on the rise and thus these patients will continue to make up a growing fraction of all patients undergoing medical imaging. In response to these findings, additional phantoms representing heavier weight percentiles can be added to the UFHADM and UFHADF patient-dependent series. These phantoms can be used to better represent the overweight population representing a considerable improvement over previous methods for dose reconstruction in radiology and fluoroscopy.

ACKNOWLEDGMENTS

This work was supported in part by Grant Nos. RO1 CA116743 and CO6 CA059267 from the National Cancer Institute and Contract No. HHS-N2612-0090-0098P from the NCI Radiation Epidemiology Branch.

[a]Author to whom correspondence should be addressed. Electronic mail: wbolch@ufl.edu; Telephone: (352) 846-1361; Fax: (352) 392-3380.

[1]W. P. Segars, D. S. Lalush, and B. M. W. Tsui, "A realistic spline-based dynamic heart phantom," IEEE Trans. Nucl. Sci. **46**, 503–506 (1999).

[2]BLENDER, http:/www.blender.org/ (2010).
[3]MAKEHUMAN, http:/makehuman.org/ (2010).
[4]C. Lee, D. Lodwick, J. Hurtado, D. Pafundi, J. L. Williams, and W. E. Bolch, "The UF family of reference hybrid phantoms for computational radiation dosimetry," Phys. Med. Biol. **55**, 339–363 (2010).
[5]V. F. Cassola, V. J. Lima, R. Kramer, and H. J. Khoury, "FASH and MASH: Female and male adult human phantoms based on polygon mesh surfaces: I. Development of the anatomy," Phys. Med. Biol. **55**, 133–162 (2010).
[6]J. Zhang, Y. H. Na, P. F. Caracappa, and X. G. Xu, "RPI-AM and RPI-AF, a pair of mesh-based, size-adjustable adult male and female computational phantoms using ICRP-89 parameters and their calculations for organ doses from monoenergetic photon beams," Phys. Med. Biol. **54**, 5885–5908 (2009).
[7]Y. H. Na, B. Zhang, J. Zhang, P. F. Caracappa, and X. G. Xu, "Deformable adult human phantoms for radiation protection dosimetry: Anthropometric data representing size distributions of adult worker populations and software algorithms," Phys. Med. Biol. **55**, 3789–3811 (2010).
[8]P. Johnson, C. Lee, K. Johnson, D. Siragusa, and W. Bolch, "Influences of patient size on dose conversion coefficients: A hybrid phantom study for adult cardiac catheterization," Phys. Med. Biol. **54**, 3613–3629 (2009).
[9]P. Johnson, S. Whalen, M. Wayson, B. Juneja, C. Lee, and W. Bolch, "Hybrid patient-dependent phantoms covering statistical distributions of body morphometry in the US adult and pediatric population," Proc. IEEE **97**, 2060–2075 (2009).
[10]R. Veit and M. Zankl, "Variation of organ doses in pediatric radiology due to patient diameter calculated with phantoms of varying voxel size," Radiat. Prot. Dosim. **49**, 353–356 (1993).
[11]C. J. Tung, C. J. Lee, H. Y. Tsai, S. F. Tsai, and I. J. Chen, "Body size-dependent patient effective dose for diagnostic radiography," Radiat. Meas. **43**, 1008–1011 (2008).
[12]M. Zankl, U. Fill, N. Petoussi-Henss, and D. Regulla, "Organ dose conversion coefficients for external photon irradiation of male and female voxel models," Phys. Med. Biol. **47**, 2367–2385 (2002).
[13]CDC, "National Health and Nutrition Examination Survey (NHANES) III," www.cdc.gov/nchs/nhanes.htm (2005).
[14]D. B. Pelowitz, Report No. LA-CP-05-0369, 2005.
[15]M. Rosenstein, O. H. Suleiman, R. L. Burkhart, S. H. Stern, and G. Willims, Report FDA Report No. 92-8282, 1992.
[16]S. H. Stern, M. Rosenstein, L. Renaud, and M. Zankl, FDA Report No. 95-8288, 1995.
[17]K. Cranley, B. J. Gilmore, G. W. A. Fogarty, and L. Desponds, Report No. 78, 1997.
[18]E. Y. Han, W. E. Bolch, and K. F. Eckerman, "Revisions to the ORNL series of adult and pediatric computational phantoms for use with the MIRD schema," Health Phys. **90**, 337–356 (2006).